# FREEZE-OUT CONDITIONS IN HEAVY ION COLLISIONS FROM 1 TO 2 AGEV [a]

BYUNGSIK HONG and THE FOPI COLLABORATION
*GSI, Planckstraße 1, D-64291, Darmstadt, Germany*
*E-mail: B.Hong@gsi.de*

The freeze-out temperature, radial flow velocity and baryon chemical potential are estimated in the context of thermal and hadrochemical equilibrium model for central $^{58}$Ni + $^{58}$Ni collisions at incident beam energies from 1 to 2 AGeV.

## 1 Introduction

One of the main purpose of present relativistic heavy ion collision experiments at the GSI SIS is to investigate the properties of hot and dense hadronic matter [1]. However most of the hadronic observables do not remember the initial conditions due to the large nuclear interaction cross sections, and reflect only the freeze-out moment. This means that the conditions of the compressed hadronic fireball can only be deduced in a model dependent way at present. On the other hand, the knowledge at freeze-out itself is important, since it gives hints on the degree of equilibration. To a large extent, a thermal and hadrochemical equilibrium model can explain the various particle spectra and yields including multistrange baryons at AGS and SPS energies [2]. In this article, we want to adopt the same idea in order to learn whether the thermodynamic equlibration is achived at incident beam energies below 2 AGeV.

Under the equilibrium model, the freeze-out condition can be described by three parameters, i.e. temperature ($T$), radial flow velocity ($\beta_r$) and baryon chemical potential ($\mu_B$). Sec. 2 explains the estimations of $T$ and $\beta_r$ from the transverse momentum ($p_t$) spectra, and Sec. 4 explains those of $T$ and $\mu_B$ from the particle yields including the $\Delta$ abundance estimated in Sec. 3. The systematic comparison of freeze-out conditions with the AGS and SPS data is given.

The experiment has been performed with 1.06, 1.45 and 1.93 AGeV $^{58}$Ni beams on the fixed $^{58}$Ni target, using FOPI detector[3]. The azimuthally symmetric forward plastic wall covers $\theta_{Lab}$ from 7 to 30 degrees, and the charged particle multiplicity distribution is used for the centrality selection. The central drift chamber covers $\theta_{Lab}$ from 30 to 150 degrees. For the particle iden-

[a] Presented in the International Research Workshop "Heavy Ion Physics at Low, Intermediate and Relativistic Energies using $4\pi$ Detectors", Poiana Brasov, Romania, October 7-14, 1996.

tification, the parameterized Bethe-Bloch formula is applied to the $dE/dx$ and momentum correlation. For the particle spectra, the normalized rapidity $y^{(0)} = y/y_{cm} - 1$ and transverse mass $m_t = \sqrt{p_t^2 + m_0^2}$, where $y_{cm}$ is the c.m. rapidity and $m_0$ is the mass of considered particle. The convention $\hbar = c = 1$ is used.

## 2 Radial Flow

The radial flow of the midrapidity fireball has been of high interest as an important energy carrier [2,4,5]. To the midrapidity spectra of high $p_t$ pions,[b] protons and deuterons for central events (upper 100mb), we apply the simple blast model assumption proposed by Siemens and Rasmussen [6]:

$$\frac{1}{m_t^2}\frac{d^2N}{dm_t dy^{(0)}} \propto \cosh y \cdot e^{-\gamma_r E/T} \cdot [(\gamma_r + \frac{T}{E})\frac{\sinh\alpha}{\alpha} - \frac{T}{E}\cosh\alpha], \qquad (1)$$

where $\gamma_r = 1/\sqrt{1-\beta_r^2}$, $\alpha = (\gamma_r \cdot \beta_r \cdot p)/T$, and $E$ and $p$ are the total energy and momentum of the particle in c.m. In this model, the thermal equilibrated system expands isotropically, and all the particles in the system are sharing the common $T$ and $\beta_r$, i.e. a shell type freeze-out scenario. The effect of the collective flow can be more significant for heavier particles as seen at lower energy [4]. However the light particles take over the role of heavy clusters at higher beam energy, and furthermore the danger for the light particles, especially $Z$ =1, at lower energy due to the evaporation from the heavier fragments is absent here.

We vary $T$ and $\beta_r$ from the model until they span our experimental data $T_B$ of three particle species simultaneously for a measured $m_t$ range. The left panel of Fig. 1 displays the range of the model calculations with data for 1.93 AGeV. Having determined $T$ and $\beta_r$, we confirm the results by comparing the Bolzmann spectra by model with data directly as shown in the right panel of Fig. 1. Table 1 summarizes $T$ and $\beta_r$ values for all three beam energies from this analysis.

Fig. 2 shows the compilation of $T$ and $\beta_r$ from the current analysis with other existing data for Au+Au using the light particles [5,7]. Firstly we find that both $T$ and $\beta_r$ increase monotonically as a function of beam energy up to 2 AGeV for both colliding systems. Secondly the temperature $T$ seems to be independent of the system size, while the radial flow velocity $\beta_r$ is larger

[b] In a Bolzmann representation, i.e. $1/m_t^2 \cdot d^2N/dm_t dy^{(0)}$ vs. $m_t - m_0$, the midrapidity spectra of protons and deuterons can be described by one exponential function with inverse slope parameter $T_B$, while those of pions require the sum of two exponential functions. For the origin of the concave shape in pion spectra, see Sec. 3.

Table 1: Summary of $T$ and $\beta_r$ for high $p_t$ pions, protons and deuterons in Ni + Ni collisions, using the shell type blast model.

| $E_{beam}/A$(GeV) | $T$ (MeV) | $\beta_r$ |
|---|---|---|
| 1.06 | 79 $\pm$ 10 | 0.23 $\pm$ 0.03 |
| 1.45 | 84 $\pm$ 10 | 0.29 $\pm$ 0.03 |
| 1.93 | 92 $\pm$ 12 | 0.32 $\pm$ 0.04 |

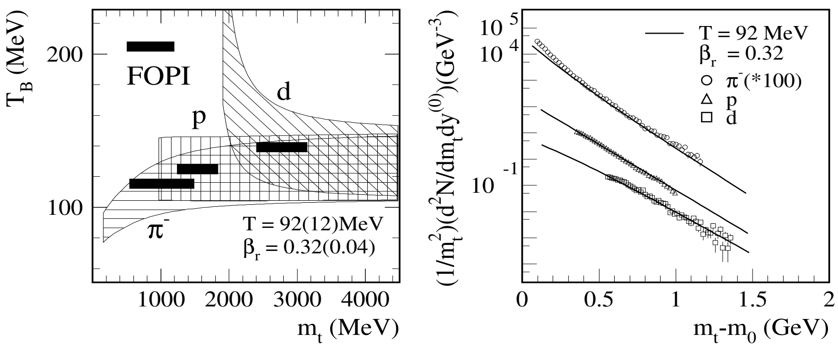


Figure 1: (Left) $T_B$ vs. $m_t$ of the model calculation spanned by the given parameters of $T$ and $\beta_r$ for $\pi^-$ (horizontally hatched), proton (vertically hatched) and deuteron (diagonally hatched) at beam energy of 1.93 AGeV. (Right) The Bolzmann spectra compared to the model calculations (solid lines). Note that the $\pi^-$ spectrum is multiplied by 100 for a clearer display.

for the larger system size (at least near 1 AGeV). Thirdly the energy partition used in the radial flow motion for a given system size ($E_{rflow}/E_{cm}$, where $E_{rflow} = (\gamma_r - 1)m_N$, $m_N$ is the nucleon mass and $E_{cm}$ is the c.m. available energy per nucleon) is fairly constant independent of the beam energies between 0.1 and 2.0 AGeV. The average value for Au+Au is at least a factor of two higher than the average of Ni + Ni data.

## 3 $\Delta$ Abundance

Charged pion spectra are interpreted using two components; the thermal pions ($\pi_T$) and the decay product of $\Delta(1232)$, simply $\Delta$ hereafter, ($\pi_\Delta$) after freeze-out. It has been demonstrated that, at the time of freeze-out, $\pi_\Delta$ contributes dominantly at the low kinetic energy part, and $\pi_T$ contributes for the

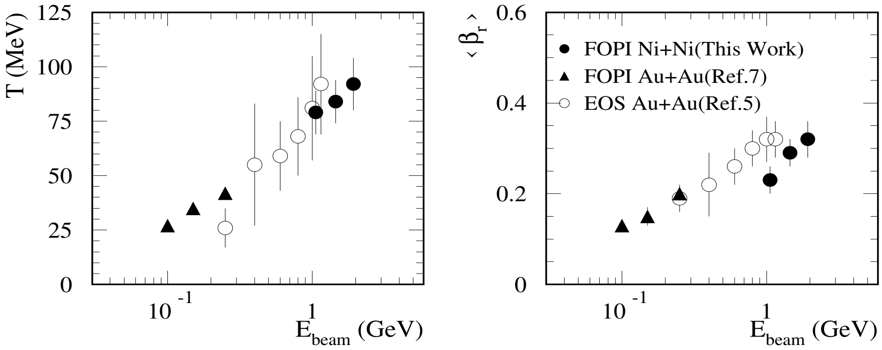


Figure 2: Compilation of $T$ (left) and $\beta_r$ (right) at different beam energies. The results obtained only with light particles are shown.

most of the high kinetic energy part of the spectra at both SIS and AGS energies [8,9]. Therefore the high $p_t$ component of the two exponential fit to the experimental pion spectra is considered as the thermal pions. For the phase space distribution of the $\Delta$ at freeze-out, the isotropic expanding blast model (Eq. 1) is employed. The parameterized relativistic Breit-Wigner form of the $\Delta$ mass distribution is also assumed [10]. The pions, which are decayed by a Monte-Carlo method from the $\Delta$ , are superposed onto the thermal pions.

The comparison of the $\pi^-$ Bolzmann spectra with the result of the model calculation is shown in Fig. 3. The overall agreement between the model and data is rather good except at the very low $m_t$ region ($m_t - m_\pi \leq 0.12$ GeV), where the data exceed the model calculations at all rapidities. In order to explain this difference, one needs to consider the effective decrease of $\Delta$ mass [8,11]. The decomposition of $\pi^-$ spectra into $\pi_T$ (dashed line) and $\pi_\Delta$ (dotted line) at midrapidity is also displayed, and it shows the low $p_t$ enhancement of the pion spectra is indeed due to the pions from $\Delta$ decay. The concave shape of the pion spectra can also be found in the cascade model like BUU [12]. The $free$ pions are originated from more energetic $\Delta$'s during the early phase of the interaction, and show a perfect exponential shape in the Bolzmann representation with a larger slope parameter than $\pi_\Delta$. However these $free$ pions need to be excluded in the estimation of $\Delta$ abundance at freeze-out in our sudden freeze-out scenario.

To estimate the yields of all pions and the low $p_t$ pions, we integrate the fitted function from $p_t = 0$ to $\infty$ for the sum of two exponentials and for

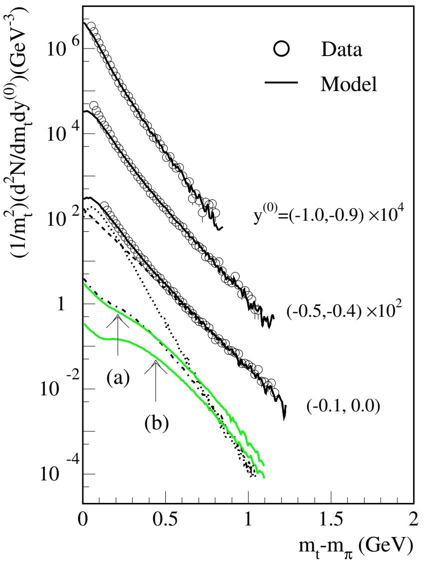


Figure 3: Bolzmann spectra of $\pi^-$ for different rapidity windows. The data are for 1.93 AGeV Ni+Ni collisions with upper 100 mb centrality cut. The black solid lines represent the model calculations including the thermal pions (dashed) as well as the pions from $\Delta$ decay (dotted). The pions from the higher baryonic resonances, e.g. $N^\star(1440)$ (dash-dotted), $N^\star(1520)$ (grey solid-a) and $N^\star(1535)$ (grey solid-b) decays, are also shown.

only low $p_t$ exponential, respectively. Since the slope parameters of the low $p_t$ exponentials agree with those of $\pi_\Delta$ spectra in the model within 6% for all beam energies, we simply take low $p_t$ pions as the total number of $\Delta$ in the system after multiplied by the proper isobaric ratio [1]. The results are summarized in Table 2 together with those at AGS energy [9]. Note that the thermal fraction of c.m. available energy to populate the estimated $\Delta$ resonance ($E_T/E_{cm}$) decreases from about 45 % to 24 % as we increase the beam energy from 1.06 to 13.6 AGeV.

Table 2: Summary of $\Delta$ abundance.

| $E_{beam}/A$ (GeV) | $n(\Delta)/n(\pi+\Delta)$(%) | $n(\Delta)/n(N+\Delta)$(%) | $E_T/E_{cm}$(%) |
|---|---|---|---|
| 1.06 | 77.4±4.0 | 10.0±2.0 | 45.3±2.8 |
| 1.45 | 68.0±3.5 | 13.1±3.3 | 41.0±3.5 |
| 1.93 | 66.4±3.4 | 17.5±4.3 | 38.3±3.8 |
| 13.6 | 33.0±5.0 | 36.0±5.0 | 24.3±3.0 |

The effect of the higher mass baryonic resonances, e.g. N$^\star$(1440), N$^\star$(1520)

and N*(1535), to our estimation of $\Delta$ and $\pi_T$ abundances has been studied within the hadrochemical equilibrium model to be explained in Sec. 4. The Bolzmann spectra of decay pions from the N*s at midrapidity are also shown in Fig. 3, after properly taking into account the branching ratios for two and three body decays. Note that the isotropic expanding blast model of primary resonances with a fixed mass has been used. The total contribution of those N*s to our $\Delta$ abundance is at most 5%, and we neglect this factor for the current analysis.

## 4 Hadrochemical Equlibrium

For an infinite volume, the particle number density in the thermal model is given by

$$\rho_i = \frac{g_i}{2\pi^2} \int_0^\infty \frac{p^2 dp}{exp((E_i - \mu_B B_i)/T_C) \pm 1}, \tag{2}$$

where $g_i$ is the spin-isospin degeneracy of particle $i$, and $E_i$ and $B_i$ are total energy in the local restframe and baryon number. In addition, we consider the correction factor [2], $f = 1 - 3\pi/4pR + 1/(pR)^2$, for a spherical volume with radius $R$ [c]. Here we use $T_C$ as a chemical freeze-out temperature in order to distinguish from the temperature by the radial flow analysis. The strangeness content has been ignored in the model. The $T_C$ and $\mu_B$ are treated as free parameters, and adjusted to describe the $p_t$ and $y$ integrated particle yields of high $p_t$ (thermal) pions, $\Delta$'s, protons, deuterons and $\eta$'s [13,14]. The comparison of the model predictions with data is shown in Fig. 4 for three incident beam energies. For the given sets of parameters, the model can reproduce the experimental data better than 20 % overall. We find that the chemical freeze-out $T_C$'s agree with the thermal freeze-out $T$'s within 8 %. The baryon freeze-out density $\rho_B$ has been estimated to be approximately 0.05-0.12/fm$^3$, which is very close to the AGS and SPS analysis [2], independent of the beam energy. On the other hand, the pion freeze-out density increases with beam energy, i.e. $\rho_\pi \approx$ 0.002-0.009, 0.005-0.013 and 0.007-0.023/fm$^3$ for 1.06, 1.45 and 1.93 AGeV, respectively. This value continues to grow to 0.09/fm$^3$ for AGS($T$ =120 MeV) and 0.3/fm$^3$ for SPS($T$ =160 MeV).

In Fig. 5, we put our experimental freeze-out points at SIS energy together with earlier estimations at AGS and SPS energies in the nuclear phase diagram [2]. Unlike the AGS and SPS points, which are close to the expected

[c]We use $R$ =5.3, 5.7 and 5.9 fm for 1.06, 1.45 and 1.93 AGeV, respectively. These values are from the coalescence analysis of deuterons. The pion HBT also gives similar results.

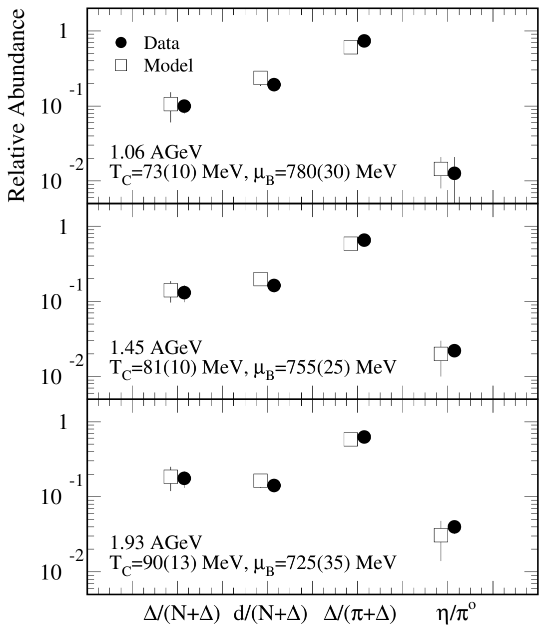


Figure 4: Comparison of the thermal model predictions (open squres) to experimental data (solid circles) for particle yield ratios at three incident beam energies. The ratios of $\eta/\pi^{\circ}$ are from the TAPS collaboration (Ref. [14]).

phase boundary between the hadron gas and quark gluon plasma, our analysis below 2 AGeV is far below the phase boundary.

Although nonstrange particles seem to fulfill the model with a thermal and hadrochemical equilibrium, the strange particles may not. To study whether the yield of strange particle is consistent with the hadrochemical equilibrium, the strange chemical potential $\mu_S$ has been determined by the measured $K^-/K^+$ ratio, which is about 3 % at 1.93 AGeV [15]. Using Eq. 2 including the strangeness part, the model predicts more than an order of magnitude larger $K^+$ yield than the measurement, $K^+/N \approx 0.11$ % [15,16]. This confirms that the strange particles are not in chemical equilibrium near threshold. However, the phase space distribution of $K^+$ is found to be consistent with the thermal equlibrium [15,16] including isotropic radial flow motion explained in Sec. 2.

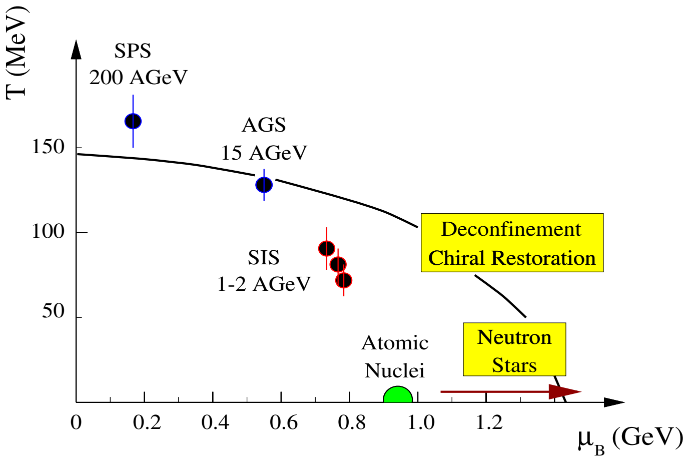

Figure 5: Phase diagram of nuclear matter and experimental freeze-out points at SIS, AGS and SPS energies.

## 5 Conclusions

We have shown that the heavy ion experimental data for nonstrange particles between 1 and 2 AGeV of the beam energy are consistent with a thermal and hadrochemical equilibrium scenario including the radial collective flow. The transverse momentum spectra of high $p_t$ pions, protons and deuterons at midrapidity require about 23 and 32 % of speed of light for the radial flow velocity in addition to the thermal motion of 79 and 92 MeV in temperature for beam energies of 1 and 2 AGeV, respectively. Both $T$ and $\beta_r$ increase monotonically as a function of beam energy up to 2 AGeV, but only the radial flow velocity shows the system size dependence, when compared to other existing data. The energy partitions used in the radial flow motion of Au+Au collisions are at least a factor of two higher than those of Ni+Ni data. The low $p_t$ enhanced part of pions decreases from 77 % to 66 % of the total pion multiplicity, while the number of nucleons excited to $\Delta$ at freeze-out increases from 10 to 18 % of all nucleons, as we increase the beam energy from 1 to 2 AGeV. The experimental freeze-out points for 1-2 AGeV are far below the phase boundary. The phase space distribution of $K^+$ is consistent with a thermal equilibrium, but the yield is more than an order of magnitude lower than the chemical equilibrium scenario.

**Acknowledgments**

We would like to thank Prof. Peter Braun-Munzinger for many helpful discussions about the thermal model.

**References**

1. R. Stock, *Phys. Rep.* **135**, 259 (1986).
2. P. Braun-Munzinger, J. Stachel, J.P. Wessels and N. Xu, *Phys. Lett.* B **344**, 43 (1995); *Phys. Lett.* B **356**, 1 (1996).
3. A. Gobbi *et al*, FOPI collaboration, *Nucl. Instrum. Methods* A **324**, 156 (1993); J.L. Ritman, *Nucl. Phys. (Proc. Suppl.)* B **44**, 708 (1995).
4. W. Reisdorf *et al*, FOPI collaboration, *Nucl. Phys.* A, (1986) in press.
5. M.A. Lisa *et al*, EOS collaboration, *Phys. Rev. Lett.* **75**, 2662 (1995).
6. P.J. Siemens and J.O. Rasmussen, *Phys. Rev. Lett.* **42**, 880 (1979).
7. G. Poggi *et al*, FOPI collaboration, *Nucl. Phys.* A **586**, 755 (1995).
8. W. Weinhold, Diploma Thesis, TH Darmstadt (1996), unpublished; W. Weinhold, B. L. Friman and W. Nörenberg, GSI Sientific Report 96-1 (1996) p. 67.
9. J. Barrette *et al*, E814 collaboration, *Phys. Lett.* B **351**, 93 (1995).
10. J.N. Ginocchio, *Phys. Rev.* C **17**, 195 (1978).
11. S.A. Bass, M. Hofmann, C. Hartnack, H. Stöcker and W. Greiner, *Phys. Lett.* B **335**, 289 (1994).
12. B.A. Li, W. Bauer, *Phys. Lett.* B **254**, 335 (1991); *Phys. Rev.* C **44**, 450 (1991).
13. B. Hong *et al*, FOPI collaboration, to be submitted to *Phys. Rev.* C.
14. F.-D. Berg *et al*, TAPS collaboration, *Phys. Rev. Lett.* **72**, 977 (1994); M. Appenheimer *et al*, GSI Sientific Report 96-1 (1996) p. 47.
15. D. Best, N. Herrmann, B. Hong, M. Kirejczyk and J. Ritman, FOPI collaboration, GSI Sientific Report 96-1 (1996) p. 49.
16. N. Herrmann, Proc. Quark Matter '96 Conference, *Nucl. Phys.* A, (1996) in press; D. Best *et al*, FOPI collaboration, to be submitted.